Analytica Chimica Acta 908 (2016) 141–149

Contents lists available at ScienceDirect

Analytica Chimica Acta

journal homepage: www.elsevier.com/locate/aca

Diamond nanoparticles as a way to improve electron transfer in sol–gel L-lactate biosensing platforms

M. Briones [a], E. Casero [a], L. Vázquez [b], F. Pariente [a], E. Lorenzo [a], M.D. Petit-Domínguez [a, *]

[a] Departamento de Química Analítica y Análisis Instrumental, Facultad de Ciencias, c/Francisco Tomás y Valiente, Nº7, Campus de Excelencia de la Universidad Autónoma de Madrid, 28049 Madrid, Spain
[b] Instituto de Ciencia de Materiales de Madrid (CSIC), c/Sor Juana Inés de la Cruz Nº3, Campus de Excelencia de la Universidad Autónoma de Madrid, 28049 Madrid, Spain

HIGHLIGHTS

- We have included for the first time diamond nanoparticles (DNPs) in a sol–gel matrix for developing lactate biosensors.
- DNPs facilitate electron-transfer within the sol–gel network in electrochemical biosensors.
- Lactate biosensors show good sensitivity, detection limit, reproducibility and stability.

GRAPHICAL ABSTRACT

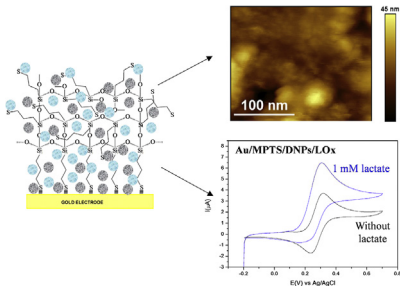

ARTICLE INFO

Article history:
Received 8 September 2015
Received in revised form
11 December 2015
Accepted 27 December 2015
Available online 5 January 2016

Keywords:
Diamond nanoparticle
Sol–gel technology
Enzymatic biosensor
Atomic force microscopy
Lactate determination

ABSTRACT

In the present work, we have included for the first time diamond nanoparticles (DNPs) in a sol–gel matrix derived from (3-mercaptopropyl)-trimethoxysilane (MPTS) in order to improve electron transfer in a lactate oxidase (LOx) based electrochemical biosensing platform. Firstly, an exhaustive AFM study, including topographical, surface potential (KFM) and capacitance gradient (CG) measurements, of each step involved in the biosensing platform development was performed. The platform is based on gold electrodes (Au) modified with the sol–gel matrix (Au/MPTS) in which diamond nanoparticles (Au/MPTS/DNPs) and lactate oxidase (Au/MPTS/DNPs/LOx) have been included. For the sake of comparison, we have also characterized a gold electrode directly modified with DNPs (Au/DNPs). Secondly, the electrochemical behavior of a redox mediator (hydroxymethyl-ferrocene, HMF) was evaluated at the platforms mentioned above. The response of Au/MPTS/DNPs/LOx towards lactate was obtained. A linear concentration range from 0.053 mM to 1.6 mM, a sensitivity of 2.6 μA mM^{-1} and a detection limit of 16 μM were obtained. These analytical properties are comparable to other biosensors, presenting also as advantages that DNPs are inexpensive, environment-friendly and easy-handled nanomaterials. Finally, the developed biosensor was applied for lactate determination in wine samples.

1. Introduction

Many types of biosensors, based on enzyme immobilization techniques, have been developed in a laboratory or even on a commercial scale for detection and control of a large number of

* Corresponding author.
E-mail address: mdolores.petit@uam.es (M.D. Petit-Domínguez).

http://dx.doi.org/10.1016/j.aca.2015.12.029
0003-2670/

analytes with important applications in health, agriculture, food industry, environmental monitoring, etc. [1]. In the last decades, several methods of enzyme immobilization have been performed, such as binding onto natural or synthetic carriers, cross-linking or inclusion in organic or inorganic polymeric network [1–3]. The recent progress in micro and nanoscale technologies opens the path to enable a number of new applications in biosensing. In this sense, nanocomposite materials prepared by the sol–gel technique in aqueous solutions appear as an appealing alternative because of their capacity to entrap enzymes without their covalent bonding to the matrix [4,5]. Thus, enzyme confinement in a sol–gel derived silicate network has been extensively studied, since enzymes remain physically encapsulated within the porous glass matrix but maintaining both their ability to interact with species that diffuse into the matrix and their native function and properties [6,7]. However, the fact that the sol–gel derived silicate network is essentially an insulating material has restricted its use for the fabrication of electrochemical sensors. Consequently, two approaches have been developed to facilitate normal electron-transfer kinetics in them [8]. In the first one, silica synthesized by a sol–gel process is post-functionalized with an electrically conductive material. For example, well-controlled chemistries for modifying a silica aerogel with RuO_2 nanoparticles, which makes a wired RuO_2 network on the silica surface, have been reported [9]. In the second approach, the conductive species is added during the silica sol–gel process and often just before silica gels [10,11]. Likewise, other variety of nanomaterials have been included in this three dimensional (3D) network in order to facilitate normal electron-transfer kinetics by acting as tiny conduction centers in sol–gel enzyme electrochemical biosensors. Particularly, gold nanoparticles have been used, due to their chemical stability and interesting physicochemical properties together with (3-mercaptopropyl)-trimethoxysilane (MPTS) sol–gel precursor [7,12]. MPTS is known to form a 3D structure plenty of thiol tail groups with a strong affinity to gold. Thanks to the thiol groups, distributed throughout the network, MPTS can be linked to the nanosized Au particles. In the same way, other carbon nanomaterials such as carbon nanotubes (which include single walled and multi-walled carbon nanotubes) [13] as well as titanium oxide nanoparticles [14] or combinations of various nanomaterials, such as multi-walled carbon nanotubes/platinum nanoparticles [15], have been used with the same purpose.

In general, we can say that sol–gel derived silicate network is an easy-handling immobilization method and a stable material that can maintain high biological activity of the enzyme and enhance the sensitivity of the biosensor. However, its cost can be more expensive, to some extent, due to the incorporation of the nanomaterials described. Since the demand for simple and inexpensive nanomaterials is ever increasing, a new member of the carbon nanomaterials family, diamond nanoparticles (DNPs), has recently gained attention. It presents some additional advantages, compared to other carbon nanomaterials, such as an excellent biocompatibility, a noncytotoxic nature, a narrow size distribution and a moderate price since it can be produced at large-scale by detonation methods. Furthermore, as a consequence of the purification procedures employed after fabrication, DNPs possess several oxygenated functional groups on their surface, including hydroxyl and carboxyl groups, which facilitate the immobilization of biomolecules [16]. In addition, several studies have also shown that, despite the great bandgap value, undoped diamond can also be considered as a potential material for electrode developing since once immobilized onto an electrode surface it enhances the electrochemical response of different redox species in solution [17,18].

The development of highly sensitive and reliable biosensing devices for the determination of L-lactate is still of great interest in several areas such as clinical diagnostics, medicine, food industry and fermentation processes. The level of L-lactate in blood is an important parameter, with normal level ranges from 0.36 to 0.75 mM [19] and its determination is of great importance in the prevention and diagnosis of a number of clinical disorders including shock respiratory insufficiencies, heart and liver diseases, patient conditions during intensive care and surgical operations process, estimation of conditions of athletes and drug toxicity tests [20–23]. In food industry it is an indicator of the fermentative process and it is related to freshness, stability and storage quality of several products such as tomato sauces, fruits, milk, juices and wine [24–26]. Among the different conventional analytical methods available for the determination of this analyte, those based on spectrophotometry and chromatographic analysis have been widely used [21,27]. However, the majority of these methods present important drawbacks such as the need of expensive equipment or time-consuming analysis due to the extensively sample pre-treatment and reagent preparation. In this sense, the development of biosensors for lactate is of considerable interest because their use implies several advantages, such as simple and direct measurements and no need of sample preparation. Nowadays, great efforts are also being devoted to use electrochemical transducers in these biosensing devices, since they present several advantages such as a low-cost instrumentation and a rapid and simple methodology, while at the same time they provide a high selectivity, inherent to the recognition element, as well as a good sensitivity supplied by the electrochemical methods. In this sense, special attention has been paid to the development of amperometric biosensors based on the use of lactacte oxidase (LOx) immobilized onto the transducer by means of different strategies [25,26,28,29].

In the present work, we have developed a new nanostructured L-lactate electrochemical biosensor denoted as Au/MPTS/DNPs/LOx. It is based on the immobilization of LOx into a 3D polymeric network generated from MPTS onto a gold surface using the sol–gel process, which also provided a 3D sol–gel silicate network for incorporation of DNPs. This new organic-inorganic hybrid material was designed with the aim of benefiting from their different components: i) a three-dimensional polymeric network that provides a biocompatible environment for enzyme protection preserving its native function and properties. In addition, MPTS presents the advantage of forming a 3D polymeric network with thiol tail groups that serve for anchoring it onto Au surfaces; ii) DNPS contributing to facilitate normal electron transfer kinetics between the electrode surface and the redox probe, with an enhancement of the oxidation/reduction current and iii) a recognition element, the enzyme, offering a high selectivity. As far as we know, this is the first sol–gel electrochemical biosensor for L-lactate determination that includes DNPs as nanomaterial.

We have also paid close attention to characterize the different biosensor construction steps as well as the resulting device. Characterization of the designed biosensor was performed using atomic force microscopy (AFM) technique for the visualization of the surface platform, providing morphological information at the nanometer level. In addition, EIS measurements were carried out in order to determine the electron transfer resistance at the electrode surface for monitoring the different steps followed in the biosensor construction. The electrochemical response of the biosensor was obtained employing an artificial mediator (hydroxymethylferrocene, HMF), whose electrochemical behavior is followed at +0.30 V. Finally, its performance was evaluated in terms of

sensitivity, detection limit and linear response.

2. Materials and methods

2.1. Reagents and materials

Diamond nanoparticles (DNPs) were obtained from SkySpring Nanomaterials, Inc (Houston, Tx). Lactate oxidase (LOx, EC 232-841-6 from Pediococcus species) lyophilized powder containing 41 units/mg solid was obtained from the Sigma Chemical Co. (St. Louis, MO). Stock solutions were prepared dissolving 1.3 mg of the LOx lyophilized powder in 250 μL of 0.1 M phosphate buffer solution (pH = 7.0), aliquoted (10 μL) and stored at −30 °C. Under these conditions the enzymatic activity remains stable for several weeks. L-(+)-lactic acid lithium salt 97%, (3-Mercaptopropyl)-trimethoxysilane, hydroxymethyl-ferrocene (HMF), potassium hexacyanoferrate (II) 3-hydrate, $K_4Fe(CN)_6$ $3H_2O$, and potassium hexacyanoferrate (III), $K_3Fe(CN)_6$ were obtained from Aldrich Chemical Co. (Milwaukee, WI). The enzymatic assay kit for lactate determination (K-LATE 07/14) was purchased from Megazyme (Ireland). Other chemicals used in this work were reagent grade quality and used as received without additional purification steps. Sodium phosphate and sodium acetate (Merck) were employed for the preparation of buffer solutions. Water was purified with a Millipore Milli-Q-System. All solutions were prepared just prior to use.

2.2. Experimental techniques

2.2.1. Atomic force microscopy (AFM) measurements

The morphological AFM studies were performed with a Nanoscope IIIa equipment (Veeco). These experiments were carried out under buffer conditions (phosphate buffer solution, 0.1 M, pH 7) in intermittent contact mode with oxide sharpened silicon nitride tips, with a spring constant of 0.24 N/m and nominal tip radius of 10 nm (Bruker). We also performed force spectroscopy measurements under buffer conditions. In these experiments the tip is fixed at a given location on the sample surface. The tip is approached towards, and then retracted from, the surface by applying a voltage ramp to the z-piezo while the tip deflection is simultaneously recorded. In this way, plots of tip deflection versus vertical z-piezo position are obtained. The approach curve obtained on a hard surface usually has two regimes: (a) the first one corresponding to the situation when the tip is far from the surface where the deflection is null (i.e., there is not any interaction between them), (b) a marked sloped region corresponding to the situation where the tip is in contact with the surface. In this last condition, as the force applied by the tip increases, the tip deflection correspondingly increases as a consequence of the repulsive force between tip and surface. In contrast, when the surface is soft, the tip can indent the surface and this zone of the curve can present curved regions or straight ones but with smaller slopes than those obtained on a hard surface. In many cases, before entering in this second repulsive regime, there is a small decrease in the deflection corresponding to the operation of attractive forces between tip and sample before the tip touches the surface. In this work, we have plotted the force curve data rather as deflection versus actual tip-surface separation. The deflection data have been normalized by taking into account that the slope of the repulsive part of the force curve has to be equal to 1 for the rigid nanodiamond surface. Then, what is plotted is, from the point of tip-sample contact, the deflection raw data, R, versus the difference between the z-piezo position and R. In this way, the situation when a rigid hard surface is reached is easily identified by the apparition of vertical straight curves. This means that despite the applied force is increased, the tip does not change its position in contact with the surface (i.e. the tip does not indent the surface). In contrast, the regimes where the curves are not vertical would correspond to the case of soft layers which the tip indents. This force curve displaying mode becomes very useful for systems such as those studied here, in which hard DNPs particles are embedded within a soft MPTS matrix. Therefore, the DNPs particles can be found at different depth levels below the sample surface. Thus, as their apparition should be indicated by the vertical straight zones, their localization is quite straightforward.

Also, Kelvin Probe Microscopy (KFM) measurements have been performed in one sample, the one formed by a MPTS plus DNPs on gold surface. These measurements were taken under ambient conditions with an Agilent 5500 Picoplus equipment. Silicon tips coated with gold nanoparticles in the 2–3 nm range (from NEXT TIP, Spain) were employed for these studies. With this technique, a map of the spatial distribution of the surface potential together with the morphological imaging can be obtained [30]. With the Agilent equipment these both mappings can be obtained simultaneously through the single-pass KFM imaging procedure [31,32]. In addition, a third image can be also obtained, that of dC/dZ, i.e. the capacitance gradient, which depends on the dielectric constant and local thickness of the sample [33]. Both the surface potential and capacitance gradient can be then used to obtain compositional contrast even of subsurface materials [34].

2.2.2. Electrochemical measurements

All electrochemical measurements were performed with an Ecochemie Autolab PGSTAT12 system (Utrecht, The Netherlands). Experiments were carried out in a three-compartment electrochemical cell with standard taper joints so that all compartments could be hermetically sealed with Teflon adapters. All potentials are reported against an Ag/AgCl (Metrohm, 3.0 M KCl) reference electrode. The auxiliary electrode was a platinum wire and modified-Au electrodes were used as the working electrode.

2.2.2.1. Electrochemical impedance spectroscopy (EIS). For EIS measurements, 0.1 M phosphate buffer, pH = 7, 0.1 M KCl, containing 10 mM $K_3Fe(CN)_6$/10 mM $K_4Fe(CN)_6$ was employed. A sinusoidal potential modulation of ±10 mV amplitude in the 10^4Hz-10^{-3}Hz (for Au/MPTS sample) or 10^4Hz−10^{-2} Hz (for Au, Au/MPTS/DNPs and Au/MPTS/DNPs/LOx samples) frequency range, spaced logarithmically (40 per 6 decades), was superimposed onto the formal potential of the redox couple, $[Fe(CN)_6]^{3-/4-}$. The electron transfer resistance (R_{ct}) values were calculated employing the corresponding Frequency Response Analysis software assuming an equivalent circuit.

2.2.2.2. Cyclic voltammetry (CV). CV was the electrochemical technique applied to study the response of the designed biosensor in the presence of HMF (which acts as soluble mediator in solution) and in the presence or absence of L-lactate. Solutions were deaerated with nitrogen gas before use, and the gas flow was kept over the solutions during experiments.

2.3. Procedures

2.3.1. Electrode conditioning

Prior to modifying the gold electrode, the surface was cleaned and activated as follows: gold electrodes were polished with 1 μm diamond paste (Buehler) and rinsed with water. Then, the electrodes were activated by holding the potential at +2.0 V for 5 s in 0.1 M H_2SO_4 and at −0.35 V for 10 s, following by potential cycling from −0.20 V to +1.5 V at 5 Vs^{-1} for 2 min. After this treatment, the cyclic voltammogram characteristic of a clean polycrystalline gold electrode was recorded (from −0.20 to +1.5 V) at 100 mV^{-1}.

2.3.2. AFM support

Gold supports employed for AFM measurements consisted of glass substrates (1.1 cm × 1.1 cm) covered with a chromium adhesion layer (1–4 nm thickness) in which a gold layer (200–300 nm thickness) was deposited (Arrandee Co. Werther, Germany).

2.3.3. Sol–gel solution preparation

The sol–gel stock solution was prepared mixing 200 μL of MPTS with 600 μL of water, 600 μL of methanol and 200 μL of 0.1 M HCl. This solution was sonicated using an Ultrasons bath (P-Selecta) for 30 min and subsequently the solution was left for 3 h at 20 °C [12].

2.3.4. Nanostructured biosensor preparation

The preparation of the biosensor was carried out by immersing the activated electrode or the AFM support in the MPTS sol–gel stock solution for an hour. MPTS sol chemisorbs on the polycrystalline Au electrode and leads to a 3D silicate network [7]. The resulting Au/MPTS system was thoroughly rinsed with water and 5 μL of the DNPs suspension in water (1 mg/mL) were dropped on this surface (or 100 μL for the AFM support) until dryness. The Au/MPTS/DNPs system was rinsed again with water and finally 5 μL of the LOx stock solution (or 100 μL for the AFM support) were dropped on this surface allowing it to dry (Au/MPTS/DNPs/LOx). In addition, for AFM topographical measurements a DNPs modified gold surface was also prepared by deposition of 100 μL of a suspension of DNPs in water (1 mg/mL) and allowing them to air-dry. Then, samples were measured both in air and in buffer conditions (phosphate buffer solution 0.1 M, pH 7) by AFM in the dynamic mode.

2.3.5. Determination of L-lactic acid in real samples

In 10.0 mL volumetric flasks, 2.0 mL of a white wine sample (purchased in a local market) were mixed with increasing volumes (0, 100, 200, 300, 400 and 500 μL) of a 0.010 M lactic acid standard solution and diluted to the mark with 0.1 M phosphate buffer (pH = 7.0) containing HMF (final concentration of HMF 1.0 mM). L-lactic acid concentration, obtained employing the developed biosensor by the described addition standard method, was compared to those obtained by a commercial enzymatic assay kit according to the manufacturer's instructions. This enzymatic assay is based on L-lactate dehydrogenase and D-glutamate-pyruvate transaminase. The NADH formed was measured by the absorbance increase at 340 nm and correlated with the L-lactic acid concentration.

3. Results and discussion

3.1. AFM characterization

In Figure S1 is shown a top-view AFM image of the surface of a layer deposit of DNPs on a gold substrate. Rounded structures are imaged on the surface with lateral sizes in the 12–25 nm range. It is observed that these structures aggregate forming larger structures, which leads to a rough surface (roughness around 17–20 nm). The particle sizes, taking into account the tip induced convolution effects, are consistent with those provided by the manufacturer.

In Figure S2 is displayed a characteristic image of the Au/MPTS system, which represents the first step in the biosensor construction. The morphology is quite different as very small granular structures, close to 10 nm wide and 0.4 nm high, are observed. Consequently, the surface becomes quite smoother (note the different z scale) with a surface roughness of just 0.2 nm.

Figure S3 presents the next step in the biosensor construction. It consists of the formation of a composite layer formed by the sol–gel MPTS and DNP structures. In this case, the surface morphology is akin to that one observed for the DNP system as rounded structures, in some cases forming larger aggregates, are also observed. In addition, the surface roughness is large, in the 20–25 nm range as in the case where only DNPs were deposited on gold. Thus, it would seem that the inclusion of DNP structures leads to rough surfaces. However, now most of the rounded structures are larger in size. Particles as large as 40–45 nm in lateral size can be found. However, it is worth noticing that just in the center of the images tiny small structures (with size around 10 nm) are also observed.

In this sample, we also performed KFM (surface potential) and dC/dZ (capacitance gradient) measurements under ambient conditions. Therefore, in this case the sample is under dried conditions. As noted above, these types of imaging are able to provide with compositional contrast when studying nanocomposite samples. As our sample composed by MPTS and DNPs on gold indeed is a nanocomposite, we use these techniques in order to be able to distinguish between its components. The corresponding morphological, surface potential and capacitance gradient images taken simultaneously on the same area of the Au/MPTS/DNPS sample are displayed in Fig. 1. The topographical image reveals rounded structures that tend to aggregate. Particularly, at the lowest locations a rather smooth and featureless surface is observed, which corresponds to the MPTS layer. The nanoparticle structures display a brighter/darker contrast in the surface potential and capacitance gradient images than that observed for the MPTS layer. Thus, these signals allow us to assess the presence of the diamond nanoparticles. In particular, there is relatively large degree of connectivity between the diamond nanoparticles likely induced by their tendency to aggregate.

The last system studied by AFM was that one including all the elements of the biosensor namely, Au substrate, MPTS, diamond nanoparticles and lactate oxidase. These studies were carried out under buffer conditions in intermittent contact mode. A typical AFM image is shown in Fig. 2. Large rounded structures, associated to the diamond nanoparticles, are observed together with smoother regions corresponding to MPTS-rich domains. Tiny rounded or globular structures are observed scattered on the surface in both types of zones, rounded and smooth ones. However, the large z-scale, of 45 nm, coming from the rough surface due to the inclusion of the diamond nanoparticles lowers the contrast to visualize them unambiguously. Thus, in the inset of the image is displayed a zoomed region taken on a smooth region where they are better distinguished. Furthermore, the surface profile corresponds to the path depicted by the dashed line in the inset. Along this profile, eight protuberances, with heights in the 1–2 nm range are clearly imaged. As this profile has been taken on a smooth region, it should correspond to a MPTS-terminated zone. Therefore, the low height values of the nanometer protuberances could correspond to individual LOx enzymes that are partially embedded in the MPTS layer.

Finally, we also performed force spectroscopy studies of all the systems in order to further characterize them. The curves displayed in Fig. 3 summarize the diversity of cases that we have found in the different systems. As explained above, we have plotted these curves as deflection versus tip-surface separation. In this way, a vertical line indicates the presence of a rigid, stiff, material, which in our case should correspond to diamond nanoparticle structures. The region of positive separation values corresponds to the situation in which the tip has not contacted the sample and, therefore, the deflection is null. The zone corresponding to negative separation values is related to indentation events of the tip on a soft surface. Separation equal to zero marks the point at which the tip first contacts the surface in all cases. Curve a displays a vertical line at

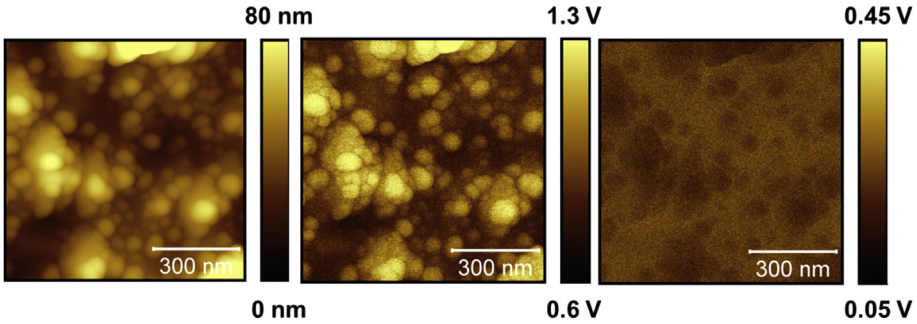

Fig. 1. 800 × 800 nm^2 AFM images of the Au/MPTS/DNPs system taken under ambient conditions: Topography (left), surface potential (middle) and capacitance gradient (right).

separation equal to zero. This curve was taken on a sample of diamond nanoparticles deposited on gold (Au/DNPs). Therefore, as the diamond surface is rigid the tip cannot indent it as it further approaches the surface. Thus, the tip displacement causes the tip deflection. Conversely, curve b, measured on the Au/MPTS sample, has not a vertical regime, in agreement with the absence of nanodiamond particles. This behavior corresponds to a situation where the tip samples a soft region and, consequently, indents it. In this region, at least 45 nm thick, the MPTS layer is being sampled. Curves c and d correspond to different zones of Au/MPTS/DNPs system. They show the same shape: first, there is a curved region for negative separation values (until 5–6 nm and 15 nm for curves c and d, respectively) to finally reach a point at which a vertical line is obtained. This behavior corresponds to a situation where the tip first samples a soft region and, consequently, indents it. However, as it further indents this soft region, it eventually reaches a stiff diamond nanoparticle (that can buried at different depths) leading to the observed vertical regime. For curve c, then, the diamond nanoparticle is 5–6 nm below the surface whereas for curve d is buried at around 15 nm of depth. Finally, curve e, measured on the Au/MPTS/DNPs/LOx sample displays the same behavior but this time the vertical curve regime is reached for separation (i.e., depth) close to 45 nm, which indicates that the diamond nanoparticle is at a deeper location. It should be noted that the depth at which DNPs are located does not depend on the presence of LOx.

Unfortunately, what we cannot assess with this analysis is whether the soft regime is due to the MPTS or to the LOx structures.

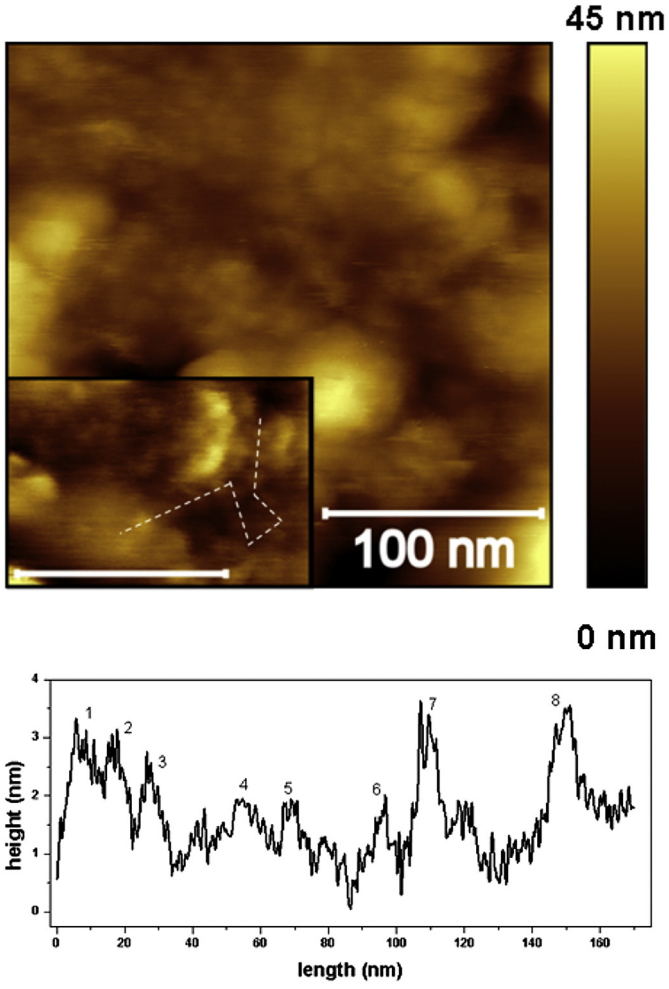

Fig. 2. 250 × 250 nm^2 AFM images of the Au/MPTS/DNPs/LOx system taken under buffer conditions in intermittent contact mode. Inset: 150 × 105 nm^2 AFM image of the same sample where small rounded structures can be observed. The surface profile (bottom) corresponds to the dashed line depicted in the inset from the top-right point to the bottom-left one. Each number in the profile indicates one of these rounded structures.

3.2. Electrochemical characterization

3.2.1. Electrochemical impedance spectroscopy

In order to study the charge transfer process occurring at the electrode interface, we have performed EIS measurements. The

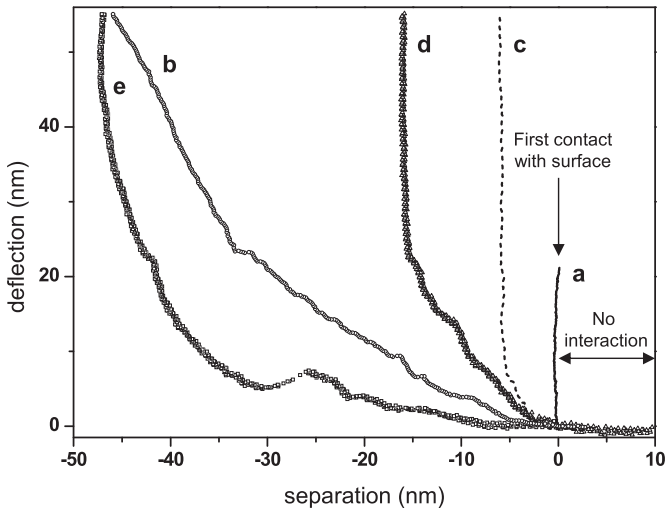

Fig. 3. Characteristic force curves depicted as deflection versus separation found in (a) Au/DNP, (b) Au/MPTS, (c, d) Au/MPTS/DNPs, (e) Au/MPTS/DNPs/LOx systems analyzed and taken under buffer conditions. The vertical curves are a fingerprint of the presence of a nanodiamond rigid structure.

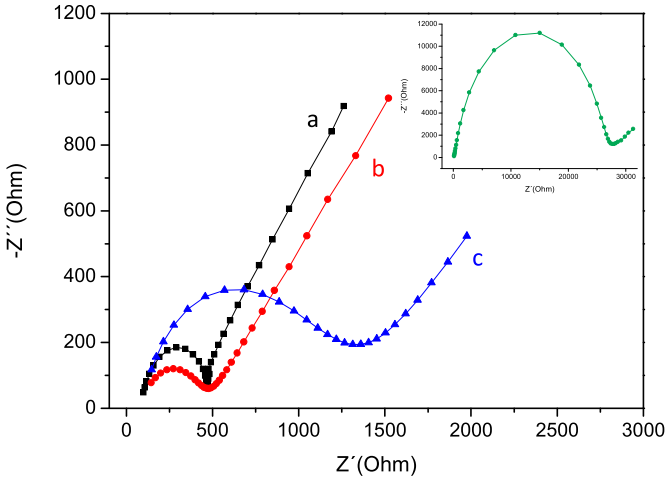

Fig. 4. Nyquist diagram for a) Au, inset) Au/MPTS, b) Au/MPTS/DNPs and c) Au/MPTS/DNPs/LOx. The solution is 0.1 M PBS (pH = 7), 0.1 M KCl containing 10 mM $K_3Fe(CN)_6$/10 mM $K_4Fe(CN)_6$.

electron-transfer resistance (R_{ct}) obtained from Nyquist plots (Fig. 4) for a bare gold electrode was 398 Ω. When the electrode is modified with MPTS, this value increases dramatically, reaching 27,900 Ω. The incorporation of diamond nanoparticles to the MPTS sol–gel matrix diminishes the electron-transfer resistance to a similar value (474 Ω) than that of the bare gold electrode, demonstrating that DNPs improve the electron transfer within sol–gel networks. For the whole system (Au/MPTS/DNPs/LOx), the R_{ct} increases again (1380 Ω) due to the relative insulating character of the enzyme.

3.2.2. Cyclic voltammetry

The electrochemical behavior of 1 mM HMF in phosphate buffer pH = 7 was first evaluated at bare gold electrode to establish a baseline for comparison with Au/MPTS, Au/MPTS/DNPs and Au/MPTS/DNPs/LOx modified electrodes. A typical cyclic voltammogram is shown in Fig. 5, curve a, for the ferrocene/ferrocinium process in aqueous media at bare gold electrode at a formal potential of +0.27 V. When the Au/MPTS electrode was immersed in an aqueous solution containing HMF, diffusion of the analyte into the sol–gel network could be observed by an increase in peak current (Fig. 5, curve b), with a higher increment of the anodic peak (1.5 times higher than the anodic peak corresponding to bare gold electrode) [35].

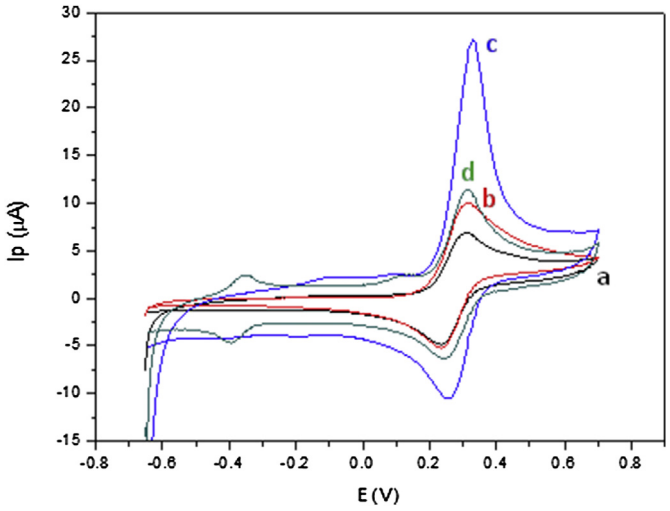

Fig. 5. Cyclic voltammograms of bare gold (a), Au/MPTS (b), Au/MPTS/DNPs (c) and Au/MPTS/DNPs/LOx (d) electrodes in 0.1 M pH = 7 phosphate buffer solution containing 1 mM of HMF. Scan rate: 100 mV s^{-1}.

In a second step, we have obtained the cyclic voltammogram of HMF at the Au/MPTS/DNPs platform (Fig. 5, curve c). As can be concluded from the comparison with the bare gold electrode, the current intensity of both anodic and cathodic peaks is clearly enhanced. In particular, anodic peak presents a peak current four times higher and almost three times higher than those of the Au and Au/MPTS platforms. This current enhancement can be explained by considering that, in addition to an increase in the relative surface area, DNPs can undergo oxidation and reduction of HMF as a consequence of the existence of DNPs surface redox states [18] and, at the same time, they act as tiny conduction centers between the HMF that has been diffused within the sol–gel matrix and the underlying electrode [12]. In a third step, the electrochemical characterization of the biosensing platform Au/MPTS/DNPs/LOx was performed under the same conditions. The resulting cyclic voltamogram (Fig. 5, curve d) shows a new pair of redox peaks, located at a formal potential of −0.4 V. This value, calculated as the average value of the oxidation and reduction peak potentials, is similar to that previously reported for other immobilized enzymes that contain the same redox active center (Flavin Adenine Dinucleotide, FAD) than lactate oxidase [36–38]. Then, the observed reversible waves can be ascribed to the direct electron transfer (DET) between the redox active center of the enzyme and the underlying electrode surface, according to:

$$\text{LOx (FAD)} + 2e^- + 2H^+ \leftrightarrow \text{LOx (FADH}_2\text{)}$$

In addition, from control experiments, it can be observed that these peaks do not appear either for a bare gold electrode or a DNPs modified gold electrode or a LOx modified Au electrode. Then, it can be concluded that the simultaneous presence of both DNPs and LOx is necessary to promote direct electron transfer between redox enzyme and the underlying electrode [18]. It is well known that the active redox center of LOx (FAD) is deeply buried in the protein shell, which makes difficult the direct electron transfer between the enzyme and the electrode, but our previous results demonstrate that the presence of the nanomaterial (DNPs) facilitates it.

3.3. Biosensor electrochemical response

Lactate biosensor is based on lactate oxidase (LOx), which in presence of oxygen catalyzes the oxidation of lactate into pyruvate and hydrogen peroxide. The activity of the immobilized LOx can be electrochemically detected by monitoring the H_2O_2 produced in the enzymatic reaction.

$$\text{Lactate} + O_2 \rightarrow \text{pyruvate} + H_2O_2$$

In order to minimize the contribution of interfering substances to the lactate biosensor response, one of the most important approaches reported in the literature is based on the replacement of the natural electron acceptor (O_2) by an artificial mediator such as hydroxymethylferrocene (HMF) to act as a redox mediator in solution. Fig. 6 (curve a) shows the cyclic voltammetric response from −0.2 V to +0.7 V at 10 mV/s for the Au/MPTS/DNPs/LOx electrode in a 0.1 M pH = 7.0 phosphate buffer solution containing 1.0 mM of HMF in the absence of lactate. Addition of lactate to a final concentration of 1.0 mM (Fig. 6, curve b) leads to an enhancement of the anodic peak current concomitant with a decrease of the cathodic peak current consistent with a clear

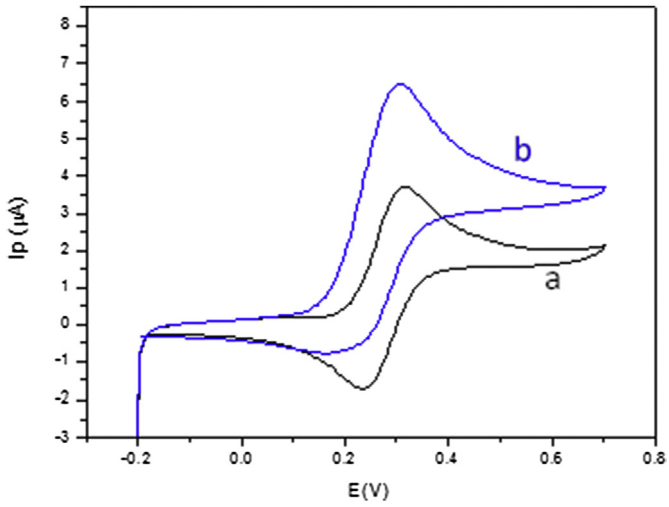

Fig. 6. Cyclic voltammetric response for Au/MPTS/DNPs/LOx platform in contact with 0.1 M pH = 7 phosphate buffer solution containing 1 mM of HMF in the absence (a), and presence (b), of 1.0 mM of lactate. Scan rate: 10 mV s^{-1}.

electrocatalytic effect. As mentioned above, we have employed diamond nanoparticles (DNPs) with the aim of improving charge transport in the designed organic-inorganic hybrid material. From comparison of the catalytic current obtained in the presence (present work) and in the absence (previous work, [12]) of DNPs, it is evident that the employment of DNPs in the biosensor construction enhances significantly the analytical response of the resulting device. On the other hand, and in order to confirm the role of the enzyme in the catalytic response, the cyclic voltammetric response of Au/MPTS/DNPs electrode in the same conditions was obtained. As one would expect, upon addition of lactate (data not shown) no catalytic waves were observed.

Analytical properties of the Au/MPTS/DNPs/LOx biosensor were obtained from the calibration curve. Fig. 7 displays a typical calibration plot obtained from the cyclic voltammetric measurements at different lactate concentrations. As shown in the inset of Fig. 7, the biosensor response was linear from 0.053 mM to 1.6 mM, with the following equation: I (μA) = 0.026 + 2.6C (mM) (R^2 = 0.991). The sensitivity, calculated from the slope of the plot, was

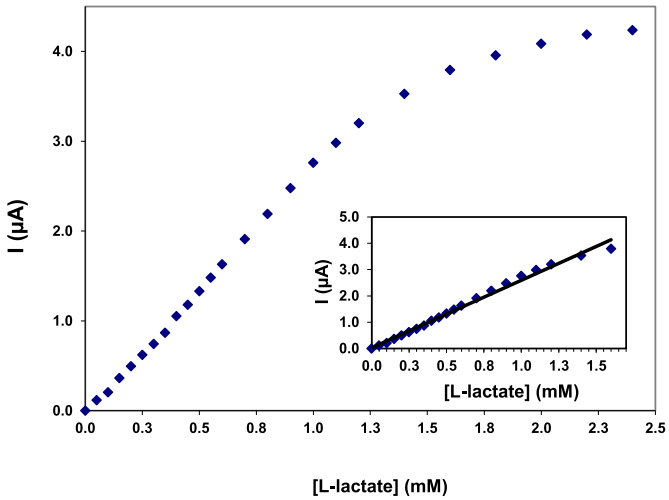

Fig. 7. Calibration curve obtained from cyclic voltammetric measurements. The inset shows the linear concentration range. Scan rate: 10 mV s^{-1}.

2.6 μA mM^{-1}. The detection limit, calculated as the ratio between three times the standard deviation of background current and the sensitivity, was 16 μM. The reproducibility was evaluated from the relative standard deviation (RSD) of three different biosensors at 0.5 mM lactate concentration level, obtaining a RSD value of 7%. Finally, the stability of biosensors was also evaluated. Firstly, we recorded successive cyclic voltammograms in 0.1 M phosphate buffer, pH 7.0, containing 0.1 mM HMF in the presence of 0.7 mM of lactate. From these measurements (Figure S4), it can be concluded that about 92% of the initial current response remains after 100 scans. In order to study the storage stability of the developed biosensor, additional experiments were carried out. Biosensors retain 100% of their initial response after 15 days of storage at 4 °C and 70% after one month, indicating that the sol–gel based biosensing platforms have an excellent storage stability.

These analytical properties are comparable to other biosensors developed in our lab for lactate determination [12,18,26,39]. In particular, comparing the performance of Au/DNPs/LOx biosensor [18] with those of Au/MPTS/DNPs/LOx, the presence of sol–gel matrix improves the stability. After the same period of time (15 days), the Au/DNPs/LOx retains the 50% of its initial response while a value of 100% is obtained for the Au/MPTS/DNPs/LOx. This result confirms that encapsulation of the enzyme in a 3D sol–gel matrix allows preserving its catalytic activity and avoids its leaking to the solution. On the other hand, as can be seen in Table 1, biosensors including different kinds of nanomaterials such as AuNPs [12] or graphene [39] lead to similar properties than those that include DNPs (present work). However, the employment of DNPs gives rise to more economic devices. In addition, DNPs are easy-handled and inexpensive candidates as nanomaterials capable of enhancing the electron transfer in sol–gel materials.

3.4. Determination of L-lactic acid in real samples

In order to demonstrate the applicability of the developed biosensor for lactic acid determination in real samples, where possible interferences due to the complexity of the matrix can occur, we have analyzed a beverage (wine) containing lactic-acid following the procedure described in the experimental section. The obtained results were compared with those obtained employing a commercial enzymatic assay kit. The average lactate concentration value obtained for three measurements using different biosensors (5.8 ± 0.2 mM) agrees well with those obtained by the enzymatic kit (5.6 ± 0.4 mM). However, the employment of the biosensor method is more rapid, direct and economical.

4. Conclusions

In the present work, we have included for the first time diamond nanoparticles in a sol–gel matrix in order to improve electron transfer in L-lactate biosensing platforms. Topographical AFM measurements demonstrate that inclusion of DNPs in the sol–gel matrix leads to rougher surfaces. Moreover, surface potential and capacitance gradient measurements allow us distinguish between the different components (MPTS, DNPs) of our nanocomposite. From force curves, it can be concluded that DNPs are buried at different depths in the sol gel 3D network. EIS measurements demonstrate that the presence of DNPs improve the electron transfer within sol–gel matrix. The developed Au/MPTS/DNPs/LOx biosensor shows a linear concentration range from 0.053 mM to 1.6 mM, a sensitivity of 2.6 μA mM^{-1}, a detection limit of 16 μM, a good reproducibility (RSD 7%) as well as an excellent stability. These analytical properties are comparable to other biosensors previously published, presenting also as advantages that DNPs are inexpensive and easy-handled nanomaterials. The developed biosensor has

Table 1
Analytical parameters of gold based biosensors. Au = gold, LOx = lactate oxidase, DTSP = 3,3′-dithiodipropionic acid di(N-succinimidyl ester), MPTS = (3-mercaptopropyl)-trimethoxysilane, AuNPs = gold nanoparticles, DNPs = diamond nanoparticles, GC = glassy carbon, GO = graphene oxide, ERG = electrochemically reduced graphene.

Reference	Electrode	Linear range (mM)	Sensitivity ($\mu A\ mM^{-1}$)	Detection limit (μM)	R.S.D. (%)
[26]	Au/LOx	Up to 0.3	0.77	10	8
[26]	Au/DTSP/LOx	Up to 0.2	0.69	40	8
[12]	Au/MPTS/AuNPs/LOx	0.05–0.25	3.4	4.0	5
[18]	Au/DNPs/LOx	0.05–0.7	4.0	15	3
[39]	GC/GO/LOx	0.018–0.58	6.5	5.5	3
[39]	GC/ERG/LOx	0.025–0.25	3.2	7.5	6
Present work	Au/MPTS/DNPs/LOx	0.05–1.6	2.6	16	7

been successfully applied to lactate determination in wine samples, demonstrating its suitability to measure this analyte in a complex matrix.

Acknowledgments

This work has been supported by Ministerio de Economía y Competitividad (Projects no. CTQ2014-53334-C2-1-R and FIS2012-38866-C05-05) and Comunidad Autónoma de Madrid (Project NANOAVANSENS S2013/MIT-3029).

Appendix A. Supplementary data

Supplementary data related to this article can be found at http://dx.doi.org/10.1016/j.aca.2015.12.029.

References

[1] B.M. Brena, F. Batista-Viera, Immobilization of enzymes, in: J.M. Guisan (Ed.), Immobilization of Enzymes and Cells, second ed.Series Methods in Biotechnology, vol. 22, Springer, 2006, pp. 15–30. Available from: http://www.springer.com/978-1-58829-290-2.
[2] I. Chibata, in: I. Chibata (Ed.), Immobilized Enzymes, John Wiley, New York, 1978, pp. 1–73.
[3] A.A. Khan, M.A. Alzohairy, Recent advances and application of immobilized enzyme technologies, Re. J. Biol. Sci. 5 (8) (2010) 565–575.
[4] G. Preda, O. Bizerea, B. Vlad-Oros, Sol-gel technology in enzymatic electrochemical biosensors for clinical analysis, in: P. Andrea Serra (Ed.), Biosensors for Health, Environment and Biosecurity, 2011, pp. 363–388. Available from: http://www.intechopen.com/books/biosensors-forhealth-environment-and-biosecurity/sol-gel-technology-in-enzymatic-electrochemical-biosensors-for-clinicalanalysis.
[5] Y.A. Shchipunova, T.Y. Karpenko, I.Y. Bakunina, Y.V. Burtseva, T.N. Zvyagintseva, A new precursor for the immobilization of enzymes inside sol–gel-derived hybrid silica nanocomposites containing polysaccharides, J. Biochem. Biophys. Methods 58 (2004) 25–38.
[6] T.M. Park, E.I. Iwuoha, M.R. Smyth, R. Freaney, A.J. Mcshane, Sol-gel based amperometric biosensor incorporating an osmium redox polymer as mediator for detection of L-lactate, Talanta (1997) 973–978.
[7] B.K. Jena, C.R. Raj, Electrochemical biosensor based on integrated assembly of dehydrogenase enzyme and gold nanoparticles, Anal. Chem. 78 (2006) 6332–6339.
[8] S.C. Warren, M.R. Perkins, A.M. Adams, M. Kamperman, A. Burns, H. Arora, E. Herz, T. Suteewong, H. Sai, Z. Li, J. Werner, J. Song, U. Werner-Zwanziger, J.W. Zwanziger, M. Grätzel, F.J. DiSalvo, U. Wiesner, A silica sol–gel design strategy for nanostructured metallic materials, Nat. Mater. 11 (2012) 460–467.
[9] J.V. Ryan, A.D. Berry, M.L. Anderson, J.W. Long, R.M. Stroud, V.M. Cepak, V.M. Browning, D.R. Rolison, C.I. Merzbacher, Electronic connection to the interior of a mesoporous insulator with nanowires of crystalline RuO_2, Nature 406 (2000) 169–172.
[10] C.A. Morris, M.L. Anderson, R.M. Stroud, C.I. Merzbacher, D.R. Rolison, Silica sol as a nanoglue: Flexible synthesis of composite aerogels, Science 284 (1999) 622–624.
[11] S. Watcharotone, D.A. Dikin, S. Stankovich, R. Piner, I. Jung, G.H.B. Dommett, G. Evmenenko, S.E. Wu, S.F. Chen, C.P. Liu, T.S. Nguyen, R.S. Ruoff, Graphene-silica composite thin films as transparent conductors, Nano Lett. 7 (2011) 1888–1892.
[12] A.M. Parra-Alfambra, E. Casero, M.D. Petit-Domínguez, M. Barbadillo, F. Pariente, L. Vázquez, E. Lorenzo, New nanostructured electrochemical biosensors based on three-dimensional (3-mercaptopropyl)-trymethoxysilane network, Analyst 136 (2011) 340–347.
[13] J. Huang, Z. Song, J. Li, Y. Yang, H. Shi, B. Wu, J. Anzai, T. Osa, Q. Chen, A highly-sensitive L-lactate biosensor based on sol–gel film combined with multi-walled carbon nanotubes (MWCNTs) modified electrode, Mater. Sci. Eng. C 27 (2007) 29–34.
[14] J. Cheng, J. Di, J. Hong, K. Yao, Y. Sun, J. Zhuang, Q. Xu, H. Zheng, S. Bi, The promotion effect of titania nanoparticles on the direct electrochemistry lactate dehydrogenase sol-gel modified gold electrode, Talanta 76 (2008) 1065–1069.
[15] J. Huang, J. Li, Y. Yang, X. Wang, B. Wu, J. Anzai, T. Osa, Q. Chen, Development of an amperometric L-lactate biosensor based on L-lactate oxidase immobilized through silica sol-gel film on multi-walled carbon nanotubes/platinum nanoparticle modified glassy carbon electrode, Mater. Sci. Eng. C 28 (2008) 1070–1075.
[16] A.M. Schrand, C. Hens, O.A. Shenderova, Nanodiamond particles: properties and perspectives for bioapplications, Crit. Rev. Solid State Mater. Sci. 34 (2009) 18–74.
[17] K.B. Holt, D.J. Caruana, E.J. Millán-Barrios, Electrochemistry of undoped diamond nanoparticles: accessing surface redox states, J. Am. Chem. Soc. 131 (2009) 11272–11273.
[18] M. Briones, E. Casero, M.D. Petit-Domínguez, M.A. Ruiz, A.M. Parra-Alfambra, F. Pariente, Lorenzo, L. Vázquez, Diamond nanoparticles based biosensors for efficient glucose and lactate determination, Biosens. Bioelectron. 68 (2015) 521–528.
[19] D. Auria, Z. Gryczynski, I. Gryczynski, M. Rosai, J.R. Lakowicz, A protein biosensor for lactate, Anal. Biochem. 283 (2000) 83–88.
[20] J.D. Artiss, R.E. Karcher, K. Cavanagh, S.L. Collins, V.J. Peterson, S. Varma, B. Zak, A liquid-stable reagent for the determination of lactic acid: application to the Hitachi 911 and Beckman CX7, Am. J. Clin. Pathol. 114 (2000) 139–143.
[21] C.I. Li, Y.H. Lin, C.L. Shih, J.P. Tsaur, L.K. Chau, Sol–gel encapsulation of lactate deshydrogenase for optical sensing of L-lactate, Biosen. Bioelectron. 17 (2002) 323–330.
[22] B.D. Malhotra, A. Chaubey, Biosensors for clinical diagnostic industry, Sens. Actuators B 91 (2003) 117–127.
[23] G.J. Kost, T.H. Nguyen, Z. Tang, Whole-blood glucose and lactate, Arch. Pathol. Lab. Med. 124 (2000) 1128–1134.
[24] M.P. Nandakumar, A.V. Lali, B. Mattiasson, On-line monitoring of glucose and/or lactate in a fermentation process using an expanded micro-be flow injection analyser, Bioseparation 8 (1999) 229–235.
[25] F. Palmisano, M. Quinto, R. Rizzi, P.G. Zambonin, Flow injection analysis of L-lactate in milk and yoghurt by on-line microdialysis and amperometric detection at a disposable biosensor, Analyst 126 (2001) 866–870.
[26] A. Parra, E. Casero, L. Vázquez, F. Pariente, E. Lorenzo, Design and characterization of a lactate biosensor base on immobilized lactacte oxidase onto gold surfaces, Anal. Chim. Acta 555 (2006) 308–315.
[27] J. Madrid, A. Martínez-Teruel, F. Hernández, M.D. Megías, A comparative study on the determination of lactic acid in silage juice by colorimetric, high-performance liquid chromatography and enzymatic methods, J. Sci. Food Agric. 79 (1999) 1722–1726.
[28] G. Aydin, S.S. Celebi, H. Özyörük, A. Yildiz, Amperometric enzyme electrode for l(+)-lactate determination using immobilized l(+)-lactate oxidase in poly(vinylferrocenium) film, Sens. Actuators B 87 (2002) 8–12.
[29] A.M. Herrero, T. Requena, A.J. Reviejo, J.M. Pingarron, Determination of l-lactic acid in yoghurt by a bienzyme amperometric graphite–teflon composite biosensor, Eur. Food Res. Technol. 219 (2004) 556–559.
[30] W. Melitz, J. Shena, A.C. Kummela, S. Lee, Kelvin probe force microscopy and its application, Surf. Sci. Rep. 66 (2011) 1–27.
[31] M. Nonnenmacher, M.P. O'Boyle, H.K. Wickramasinghe, Kelvin probe force microscopy, Appl. Phys. Lett. 58 (1991) 2921–2923.
[32] Keysight Technologies, Compositional mapping of materials with single-pass Kelvin force microscopy, Appl. Note, http://literature.cdn.keysight.com/litweb/pdf/5990-5480EN.pdf.
[33] M.J. Cadena, R. Misiego, K.C. Smith, A. Avila, B. Pipes, R. Reifenberger, A. Raman, Sub-surface imaging of carbon nanotube–polymer composites using dynamic AFM methods, Nanotechnology 24 (2013) 135706.
[34] O.A. Castañeda-Uribe, R. Reifenberger, A. Raman, A. Avila, Depth-sensitive subsurface imaging of polymer nanocomposites using second harmonic kelvin probe force microscopy, ACS Nano 9 (2015) 2938–2947.
[35] M.D. Petit-Dominguez, H. Shen, W.R. Heineman, C.J. Seliskar, Electrochemical behavior of graphite electrodes modified by spin-coating with sol–gel-entrapped ionomers, Anal. Chem. 69 (1997) 703–710.

[36] M. Wooten, S. Karra, M. Zhang, W. Gorski, On the direct electron transfer, sensing, and enzyme activity in the glucose oxidase/carbon nanotubes system, Anal. Chem. 86 (2014) 752–757.
[37] L. Zhu, L. Xu, L. Tan, H. Tan, S. Yang, S. Yao, Direct electrochemistry of cholesterol oxidase immobilized on gold nanoparticles-decorated multi-walled carbon nanotubes, Talanta 106 (2013) 192–199.
[38] D. Wang, L. Chen, Facile direct electron transfer in glucose oxidase modified electrodes, Electrochim. Acta 54 (2009) 4316–4320.
[39] E. Casero, C. Alonso, L. Vázquez, M.D. Petit-Domínguez, A.M. Parra-Alfambra, M. de la Fuente, P. Merino, S. Álvarez-García, A. de Andrés, F. Pariente, E. Lorenzo, Comparative response of biosensing platforms based on synthesized graphene oxide and electrochemically reduced graphene, Electronalysis 25 (2013) 154–165.